Unraveling the structure of functional materials by EXAFS spectroscopy and reverse Monte Carlo simulations

Alexei Kuzmin

[1] Institute of Solid State Physics, University of Latvia, Riga, Latvia

[2] International Research Organization for Advanced Science and Technology (IROAST), Kumamoto University, Kumamoto, Japan

E-mail: a.kuzmin@cfi.lu.lv

Internet: www.dragon.lv/exafs

The 4th FRIMS International Symposium on Frontier Materials, FRIMS, NITech, Nagoya, Japan
8-9 March 2022

EXAFS Spectroscopy Laboratory

www.dragon.lv/exafs

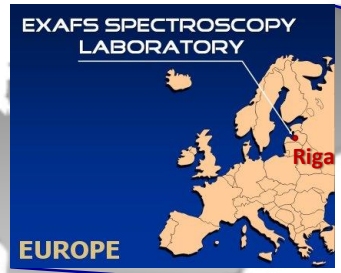

Institute of Solid State Physics
University of Latvia

Nagoya Institute of Technology

Frontier Research Institute for Materials Science

Talk outline

- **Introduction to X-ray Absorption Spectroscopy (XAS)**
  - Effect of disorder & multiple-scattering
- **Reverse Monte Carlo (RMC) simulations of EXAFS spectra**
  - Capabilities and limitations
- **Applications of the RMC-EXAFS method**
  - Thermochromic materials
  - High-Entropy Alloys
- **Conclusions**

X-ray Absorption Spectroscopy (XAS)

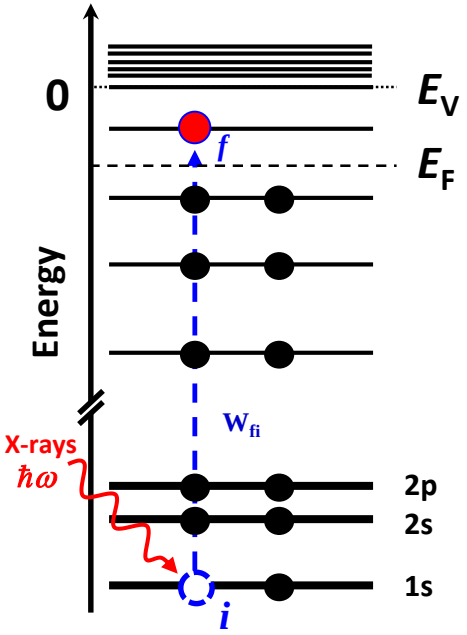

Fermi's Golden Rule:

$$\mu(E) \propto \sum_f \left|\langle f|\hat{\mathbf{H}}|i\rangle\right|^2 \delta(E_f - E_i - \hbar\omega)$$

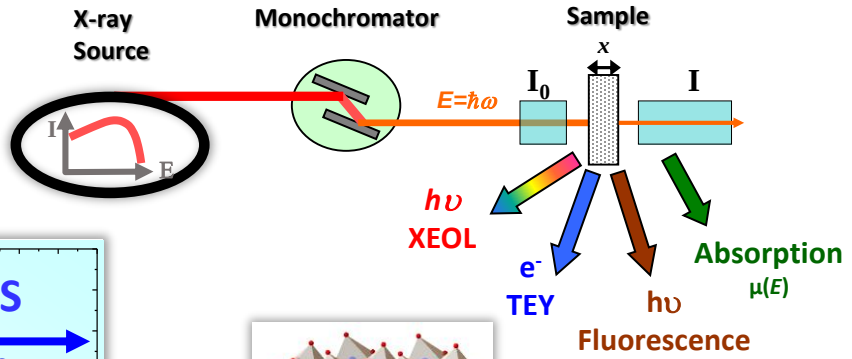

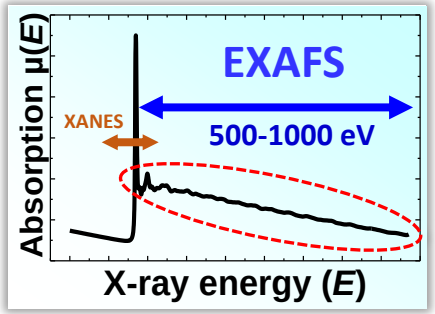

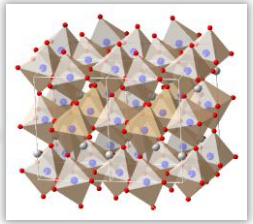

Characteristic time of X-ray absorption process:
$t_{ab} \sim 10^{-15}$-10^{-16} s

Characteristic time of thermal vibrations:
$t_{th} \sim 10^{-13}$-10^{-14} s

Atoms are frozen during X-ray absorption event

$$\mu(E) = \frac{1}{x}\ln\left(\frac{I_0(E)}{I(E)}\right)$$

$$\mu(E) \propto \frac{I_{fluo}(E)}{I_0(E)}$$

$$\mu(E) \propto \frac{I_{TEY}(E)}{I_0(E)}$$

$$\mu(E) \propto \frac{I_{XEOL}(E)}{I_0(E)}$$

Origin of Extended X-ray Absorption Fine Structure (EXAFS)

Fermi's Golden Rule: $\mu(E) \propto \sum_f \left|\langle f|\hat{\mathrm{H}}|i\rangle\right|^2 \delta(E_f - E_i - \hbar\omega) = \mu_0(E)[1 + \chi(E)]$

Dipole approximation: $\hat{H} = \hat{\epsilon} \cdot \vec{r}$

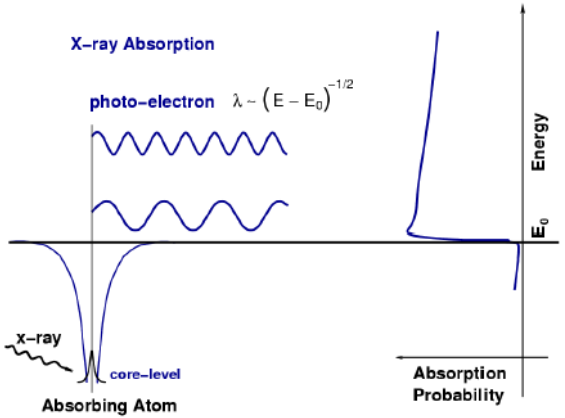

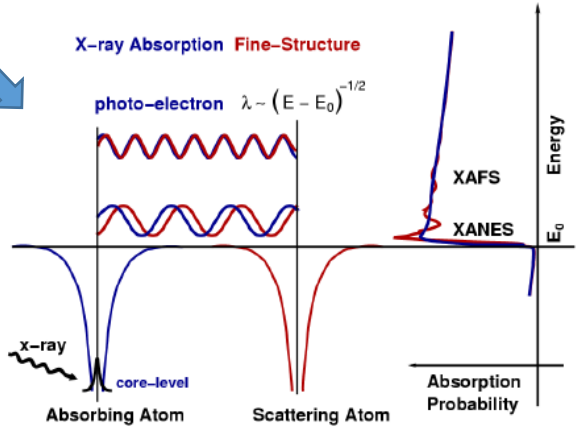

X-ray absorption through the photoelectric process.

When an X-ray has the energy of a tightly bound core electron level, E_0, the probability of absorption has a sharp rise. In the absorption process, the tightly bound corelevel is destroyed, and a photo-electron is created. The photo-electron travels as a wave with wave number *k*

$$k = 2\pi / \lambda = [(2m_e/\hbar^2)(E - E_0)]^{1/2}$$

Origin of (E)XAFS.

EXAFS occurs because the photo-electron can scatter from a neighboring atom. The scattered photo-electron can return to the absorbing atom, modulating the amplitude of the photo-electron wave-function at the absorbing atom. This in turn modulates the X-ray absorption coefficient μ(*E*), causing the EXAFS.

Multiple-scattering approach to EXAFS χ(k)

1. Multiple-scattering (MS) expansion (FEFF code):

$$\chi(k) = \sum_{n=2}^{\infty} \chi_n(k), \quad \chi_n(k) = \sum_i A_n^l(k, R_i) \sin\left(2kR_i + \phi(k, R)\right) \exp\left(-2k^2\sigma_i^2\right)$$

MS order

"Radial" disorder

J.J. Rehr, J.J. Kas, M.P. Prange, A.P. Sorini, Y. Takimoto, F. Vila, C. R. Physique 10 (2009) 548.

2. N-body expansion (GNXAS code):

$$\begin{aligned}
\chi(k) \;=\; & \int 4\pi R^2 \rho\, g_2(R)\left(\chi_2^{oio}(k) + \chi_4^{oioio}(k) + \ldots\right)\mathrm{d}R \\
& + \iiint 8\pi^2 R_1^2 R_2^2 \sin(\theta)\rho^2 g_3(R_1, R_2, \theta) \\
& \times\left(2\chi_3^{oijo}(k) + 2\chi_4^{oiojo}(k) + \chi_4^{oijio}(k) + \chi_4^{ojijo}(k) + \ldots\right)\mathrm{d}R_1\mathrm{d}R_2\mathrm{d}\theta \\
& + \iiiint 8\pi^2 R_1^2 R_2^2 R_3^2 \sin(\theta)\rho^3 g_4(R_1, R_2, \theta, R_3, \Omega) \\
& \times\left(2\chi_4^{oijko}(k) + 2\chi_4^{oikjo}(k) + 2\chi_4^{ojiko}(k) + \ldots\right)\mathrm{d}R_1\mathrm{d}R_2\mathrm{d}\theta\mathrm{d}R_3\mathrm{d}\Omega \\
& + \ldots
\end{aligned}$$

A. Filipponi, A. Di Cicco, C. R. Natoli, Phys. Rev. B 52 (1995) 15122-15134.

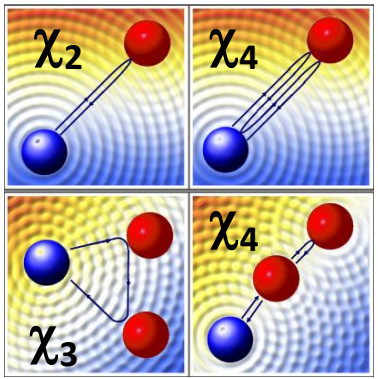

Analysis of EXAFS spectra using the Fourier filtering procedure

Strictly valid for the first peak!

$$FT(R) = \sqrt{\frac{2}{\pi}} \int_{k_{min}}^{k_{max}} \chi(k) k^n W(k) e^{-2ikR} dk$$

$$\chi_{1st\ shell}(k) \equiv BFT(k) = \frac{1}{k^n W(k)} \sqrt{\frac{2}{\pi}} \int_{R_{min}}^{R_{max}} FT(R) e^{2ikR} dR$$

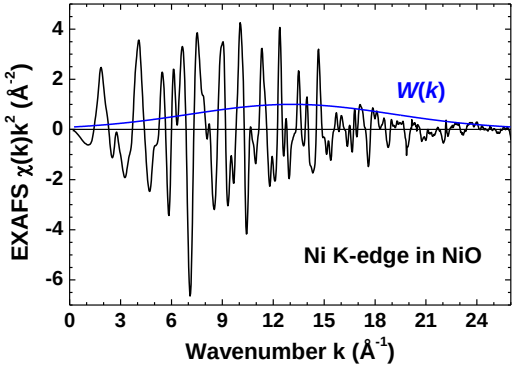

The experimental Ni K-edge EXAFS $\chi(k)k^2$ of crystalline NiO (black line) and the window function $W(k)$ (blue line).

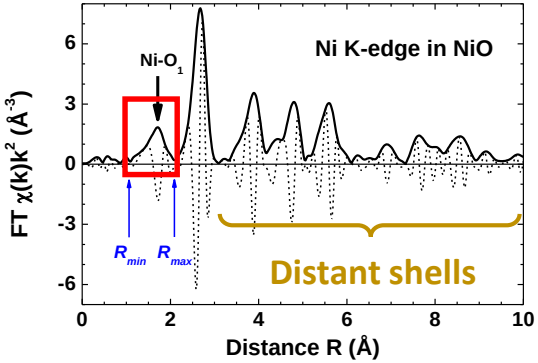

Fourier transform of the EXAFS $\chi(k)k^2$. Both the modulus (solid line) and imaginary (dashed line) parts are shown. The peak at R=1.7 Å corresponds to the first coordination shell of nickel, which is composed of six oxygen atoms in NiO.

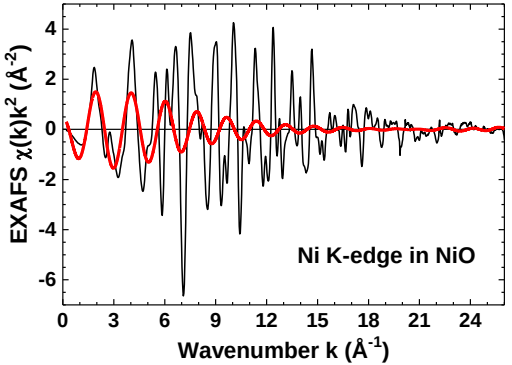

The experimental Ni K-edge EXAFS $\chi(k)k^2$ of crystalline NiO (black line) and the first shell contribution (red line).

EXAFS analysis in the single-scattering approximation

Gaussian (harmonic) model:

$$\chi_2(k) = S_0^2 \boldsymbol{N} \frac{|f_{eff}(k,R)|}{k\boldsymbol{R}^2} e^{-2\boldsymbol{R}/\lambda(k)} \sin(2k\boldsymbol{R} + \phi(k,R)) e^{-2k^2\boldsymbol{\sigma}^2}$$

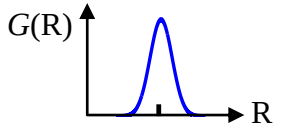

D.E. Sayers, E.A. Stern, F.W. Lytle, Phys. Bev. Lett. 27 (1971) 1204.

Cumulant (anharmonic) model:

$$\chi_2(k) = S_0^2 \boldsymbol{N} \frac{|f_{eff}(k,R)|}{k\boldsymbol{R}^2} e^{-2\boldsymbol{R}/\lambda(k)} \sin\left(2k\boldsymbol{R} - \frac{4}{3}\boldsymbol{C_3}k^3 + \phi(k,R)\right) e^{-2k^2\boldsymbol{\sigma}^2 + \frac{2}{3}\boldsymbol{C_4}k^4}$$

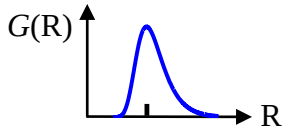

G. Bunker, Nucl. Instrum. Methods 207 (1983) 437.

General RDF model:

$$\chi_2(k) = S_0^2 \int_{R_{min}}^{R_{max}} \boldsymbol{G(R)} \frac{|f_{eff}(k,R)|}{kR^2} e^{-2R/\lambda(k)} \sin(2kR + \phi(k,R)) dR$$

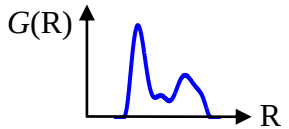

Regularization method: Yu.A. Babanov et al., Phys. Stat. Solidi (B) 105 (1981) 747.

EXAFS challenges: analysis of distant coordination shells

1 The analysis of the distant coordination shells must take into account the multiple-scattering (MS) and disorder effects.

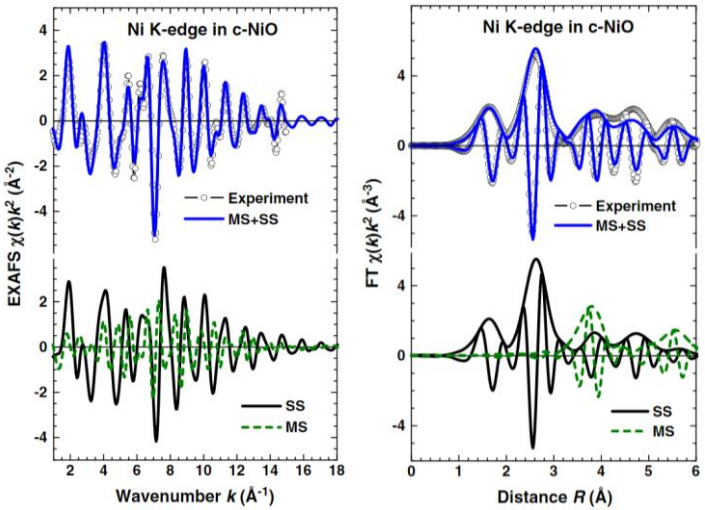

A. Anspoks and A. Kuzmin,
J. Non-Cryst. Solids 357 (2011) 2604.

NiO

Space group Fm-3m
a_0= 4.1773 Å

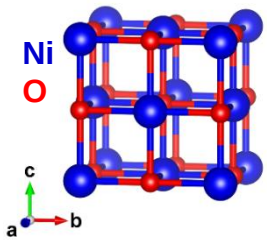

2 A number of parameters in the model increases rapidly upon an increase of analyzed region size around the absorbing atom.

This problem is especially relevant for disordered and nanocrystalline materials.

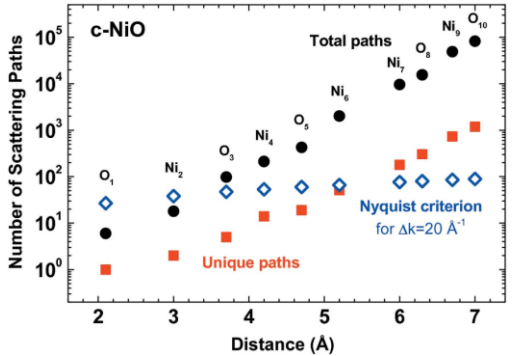

Number of scattering paths vs independent parameters N_{par}:

$$N_{\mathrm{par}} = \frac{2\Delta k \Delta R}{\pi}$$

A. Kuzmin and J. Chaboy, IUCrJ 1 (2014) 571.

Advanced methods of XAS analysis using atomistic simulations

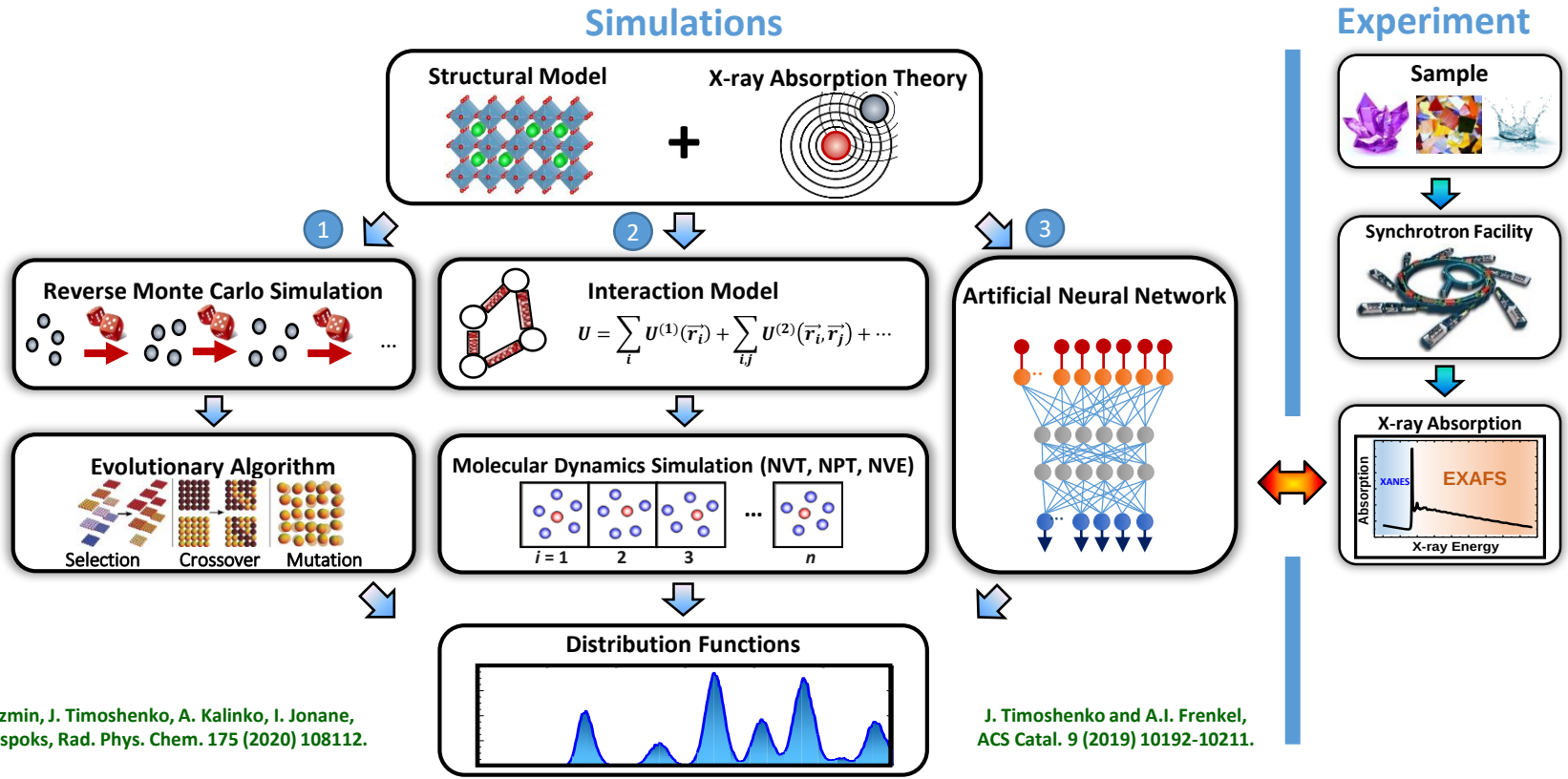

A. Kuzmin, J. Timoshenko, A. Kalinko, I. Jonane, A. Anspoks, Rad. Phys. Chem. 175 (2020) 108112.

J. Timoshenko and A.I. Frenkel, ACS Catal. 9 (2019) 10192-10211.

Reverse Monte Carlo simulations of EXAFS spectra (RMC-EXAFS)

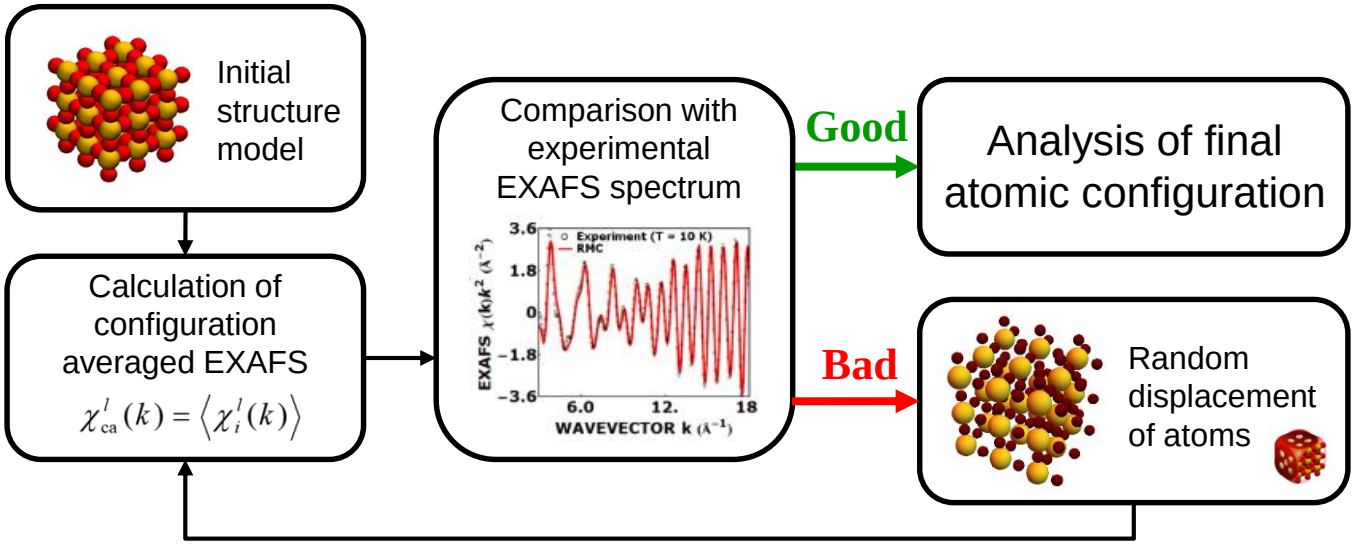

R.L. McGreevy and L. Pusztai, Mol. Simul. 1 (1988) 359.
S.J. Gurman and R.L. McGreevy, J. Phys.: Condens. Matter 2 (1990) 9463-9473.

RMC-EXAFS approach: History

Reverse Monte Carlo simulation for the analysis of EXAFS data

S J Gurman† and R L McGreevy‡
† Department of Physics, University of Leicester, Leicester LE1 7RH, UK
‡ Clarendon Laboratory, Parks Road, Oxford OX1 3PU, UK

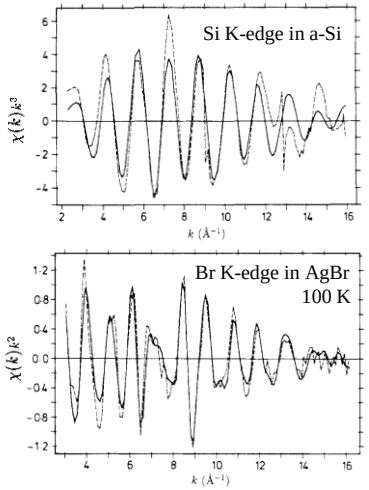

High temperature EXAFS experiments on liquid KPb alloys analysed with the reverse Monte Carlo method

W. Bras [a,b,*], R. Xu [c], J.D. Wicks[d,1], F. van der Horst [c], M. Oversluizen [a,b], R.L. McGreevy [c], W. van der Lugt [c]
[a] Netherlands Organisation for Scientific Research (NWO), The Netherlands
[b] SERC Daresbury Laboratory, Warrington WA4 4AD, UK
[c] Laboratory for Solid State Physics, Groningen University, Nijenborgh 18, 9747 AG Groningen, The Netherlands
[d] Clarendon Laboratory, Parks Road, Oxford, OX1 3PU, UK
[1] Studsvik Neutron Research Laboratory, Uppsala University, S-611 82 Nyköping, Sweden

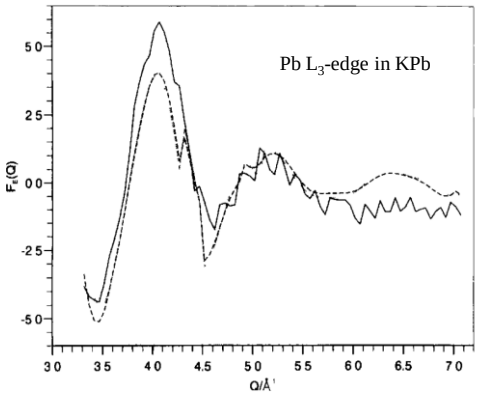

Fig. 4. EXAFS data, $F_E(Q)$, for molten KPb (solid line) compared to the RMC fit with 100% Zintl ions maintained (dotted line)

Modelling the Structure and Ionic Conduction of $(AgI)_x(AgPO_3)_{1-x}$ Glasses

J. D. Wicks,[1] L. Börjesson,[2] G. Bushnell-Wye,[3] W. S. Howells[4] and R. L. McGreevy[5]
[1] Department of Physics and Astronomy, University College London, Gower Street, London WC1E 6BT, U.K.
[2] Department of Physics, Royal Institute of Technology, S-100 44 Stockholm, Sweden
[3] SRS Daresbury Laboratory, Warrington, Cheshire WA4 4AD, U.K.
[4] ISIS Science Division, Rutherford Appleton Laboratory, Chilton, Didcot, Oxon OX11 0QX, U.K.
[5] Studsvik Neutron Research Laboratory, S-611 82 Nyköping, Sweden

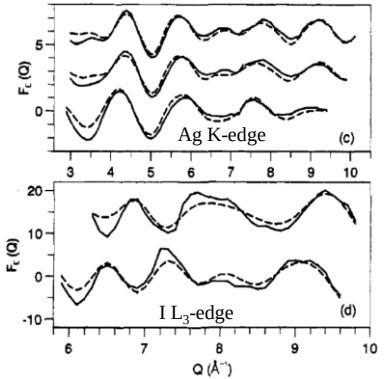

Experimental data (solid curves) and RMC fits (broken curves) for $(AgI)_x(AgPO_3)_{1-x}$ (top to bottom) x = 0.5, 0.3 and 0.0. EXAFS at (c) the Ag K-edge and (d) the I L_3-edge.

[1] S.J. Gurman and R.L. McGreevy, J. Phys.: Condens. Matter 2 (1990) 9463-9473.
[2] W. Bras, R. Xu, J.D. Wicks, F. van der Horst, M. Oversluizen, R.L. McGreevy, W. van der Lugt, Nucl. Instrum Meth. Phys. Res. A 346 (1994) 394-398.
[3] J.D. Wicks, L. Borjesson, G. Bushnell-Wye, W.S. Howells, R.L. McGreevy, Physica Scripta. T57 (1995) 127-132.

Reverse Monte Carlo method with Evolutionary Algorithm

EvAX code was developed by Dr. Janis Timoshenko

J. Timoshenko, A. Kuzmin, J. Purans, J. Phys.: Condens. Matter 26 (2014) 055401.
J. Timoshenko, A. Kuzmin, J. Purans, Comp. Phys. Commun. 183 (2012) 1237-1245.

Simulation-based analysis of EXAFS data for crystalline and nanocrystalline materials

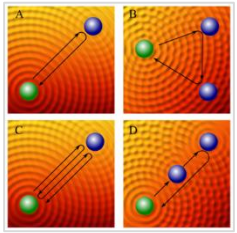

Multiple-scattering approximation

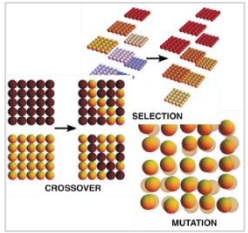

Evolutionary algorithm for optimization

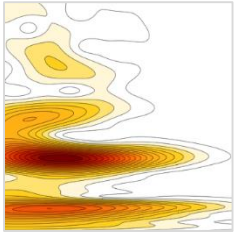

Wavelet transform for spectra comparison in k and R space

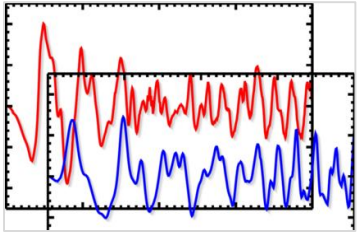

Analysis of EXAFS at several edges

Reliable analysis of distant shells, PDF and BADF

Fast with good convergence

More reliable solution

Single structural model

http://www.dragon.lv/evax/

Applications of the RMC-EXAFS method to

- Thermochromic materials
- High-Entropy Alloys

Functional Material: Copper Molybdate ($CuMoO_4$)

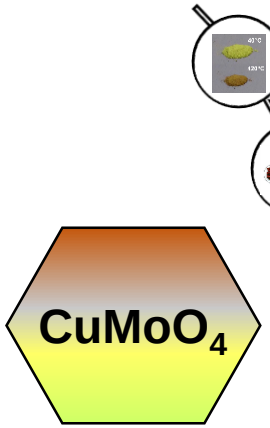

- **Thermochromic** — T. G. Steiner, et al., J. Anal. Chem. 370 (2001) 731; M. Gaudon, et al., Inorg. Chem. 46 (2007) 10200–10207; I. Yanase, et al., Ceram. Int. 39 (2013) 2059-2064; L. Robertson, et al., J. Mater. Chem. C 3 (2015) 2918-2924; N. Joseph, et al. Appl. Mater. & Interf. 12.1 (2020) 1046-1053
- **Piezochromic** — M. Wiesmann, et al., J. Solid State Chem. 132 (1997) 88-97; F. Rodríguez, et al., Phys. Rev. B 61 (2000) 16497; M. Gaudon et al., Adv. Mater.19 (2007) 3517; L. Robertson, et al., J. Mater. Chem. C 3 (2015) 2918-2924
- **Halochromic (pH)** — K. S. Makarevich, et al., Inorg. Mater. 46 (2010) 1359-1364
- **Thermosalient effect** — L. Robertson, et al., J. Mater. Chem. C 3 (2015) 2918-2924
- **Catalytic** — T.K. Ghorai et al., Mater. Res. Bull. 43 (2008) 1770; K. S. Makarevich, et al., Inorg. Mater. 46 (2010) 1359; P. Chigrin, et al., Kinetics and Catalysis 54 (2013) 76-80
- **Antibacterial** — D. Tanasic, et al., Biointerphases 12 (2017) 05G607

Thermochromic properties of $CuMoO_4$

Low Temperatures ⇒ Hysteretic Phase Transition

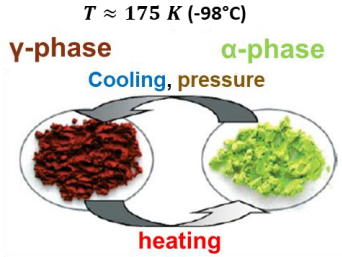

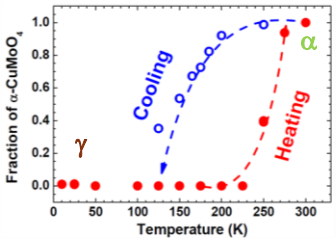

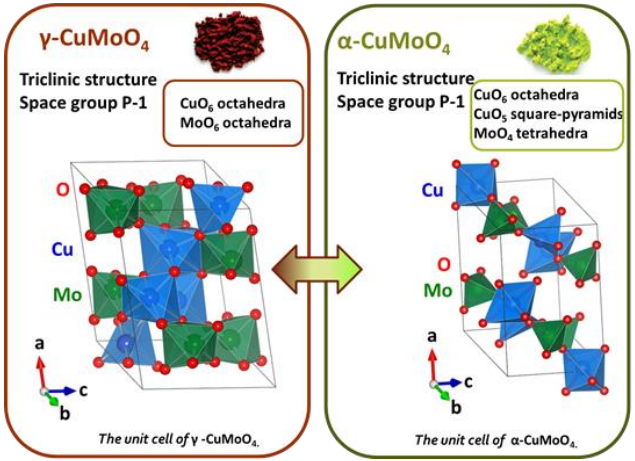

$CuMoO_4$	Phase transition T
α -> γ	120-200 K
γ -> α	230-280 K

High Temperatures

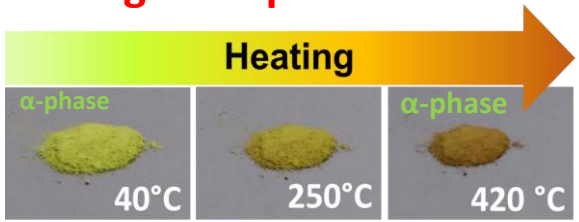

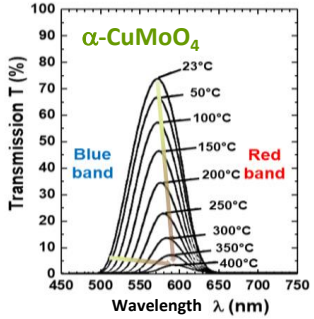

Blue band models
$O^{2-} \rightarrow Cu^{2+}$
$O^{2-} \rightarrow Mo^{6+}$
$Cu^{2+} \rightarrow Mo^{6+}$
charge transfer processes

Red band models
Cu^{2+} d-d transitions
Cu^{2+} $3d^9 \rightarrow 4p$

T. G. Steiner, et al., J. Anal. Chem. 370 (2001) 731.
M. Gaudon, et al., Inorg. Chem. 46 (2007) 10200-10207.
I. Yanase, et al., Ceram. Int. 39 (2013) 2059-2064.
L. Robertson, et al., J. Mater. Chem. C 3 (2015) 2918-2924.
N. Joseph, et al. Appl. Mater. & Interf. 12.1 (2020) 1046-1053.

Low-temperature thermochromic phase transition in γ-$CuMoO_4$

Experimental EXAFS spectra show significant differences between α un γ phases.

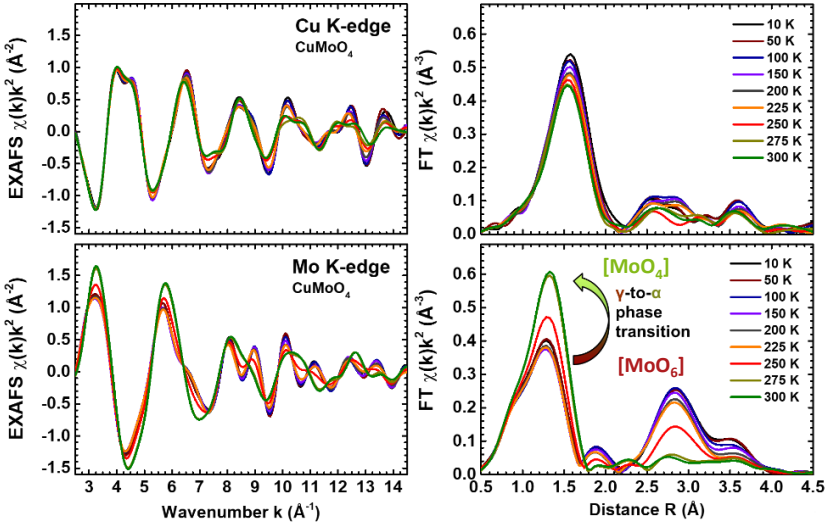

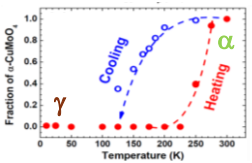

Selected results of RMC simulations at the Cu and Mo K-edges.

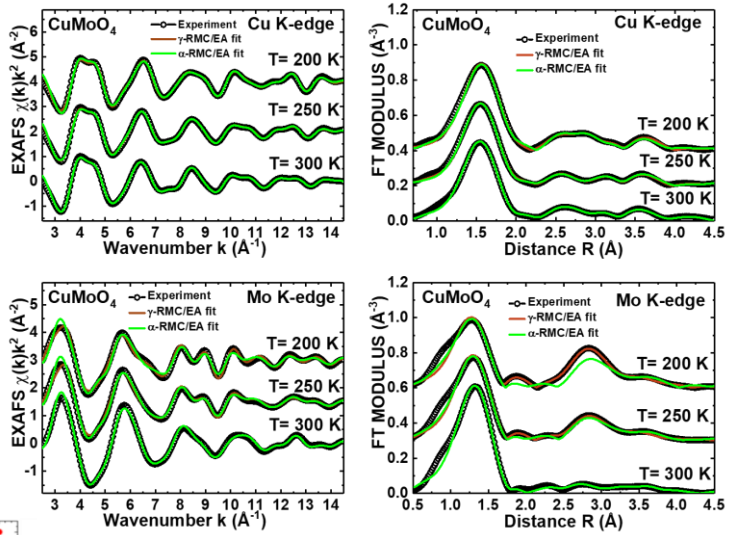

At T=250 K two phases coexist.

I. Jonane, A. Cintins, A. Kalinko, R. Chernikov, A. Kuzmin, Rad. Phys. Chem. 175 (2020) 108112.

Low-temperature thermochromic phase transition in γ-$CuMoO_4$

RMC/EA modelling allows one to follow the variation of local environment in low-symmetry structures as $CuMoO_4$ on temperature.

Information about the local environment around selected atoms in the first coordination shell.

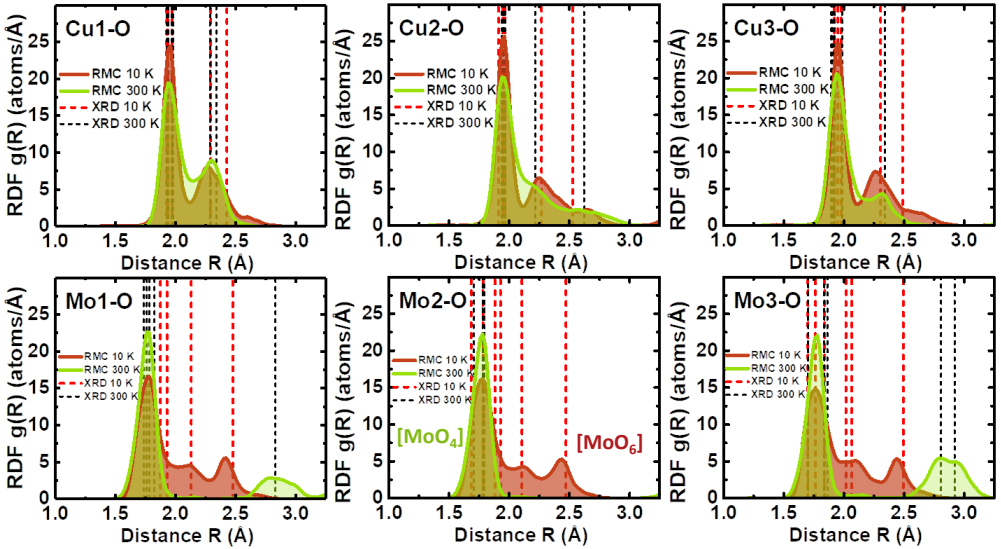

Different types of distortions of metal-oxygen octahedra reflected by Bond Angle Distribution Functions (BADFs).

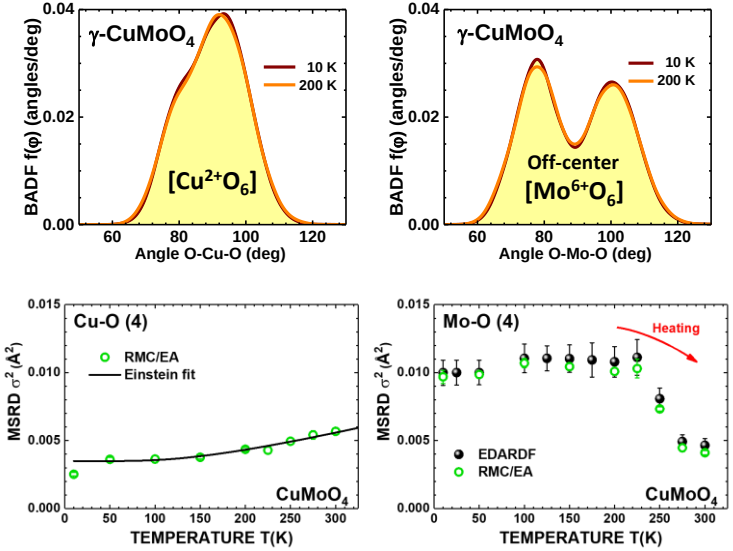

I. Jonane, A. Cintins, A. Kalinko, R. Chernikov, A. Kuzmin, Rad. Phys. Chem. 175 (2020) 108112.

High-temperature thermochromic behaviour in α-$CuMoO_4$

Rare temperature dependence of XANES region at the Cu K-edge is observed.

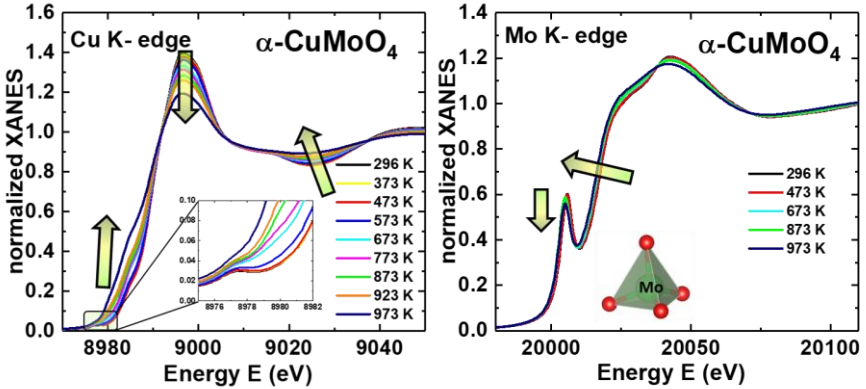

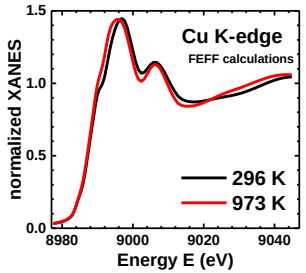

FMS calculations by the FEFF code show only the effect of the lattice constant variation.

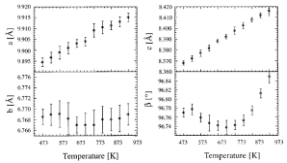

M. Wiesmann, et al., J. Solid State Chem. 132 (1997) 88-97.

There is no phase transition: α-$CuMoO_4$.

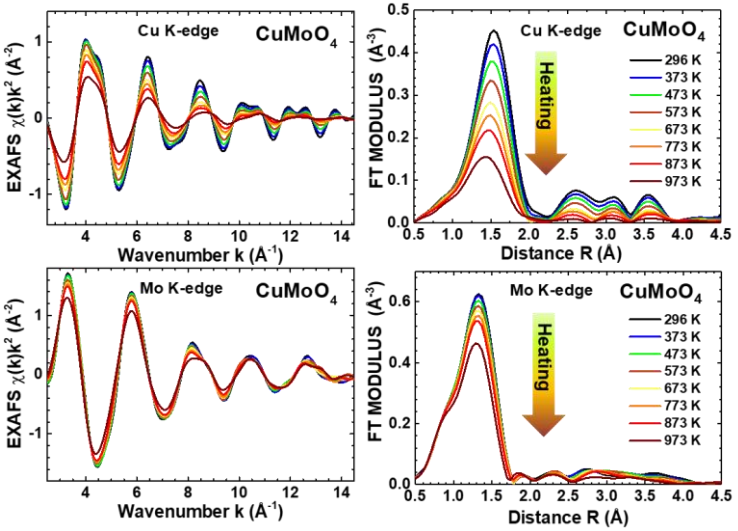

Always [MoO_4]!

I. Jonane, A. Anspoks, G. Aquilanti, A. Kuzmin, Acta Mater. 179 (2019) 26-35.

High-temperature thermochromic behaviour in α-$CuMoO_4$

Average Wyckoff positions calculated for RMC structure models are close to those of XRD.

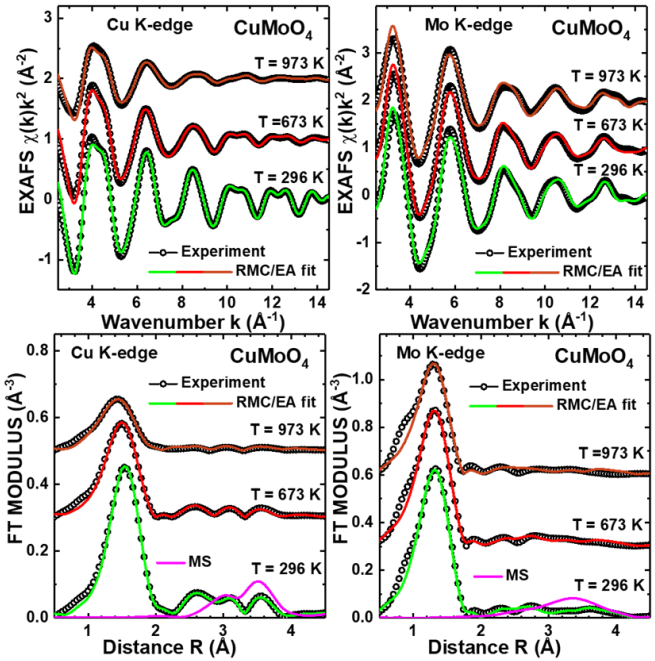

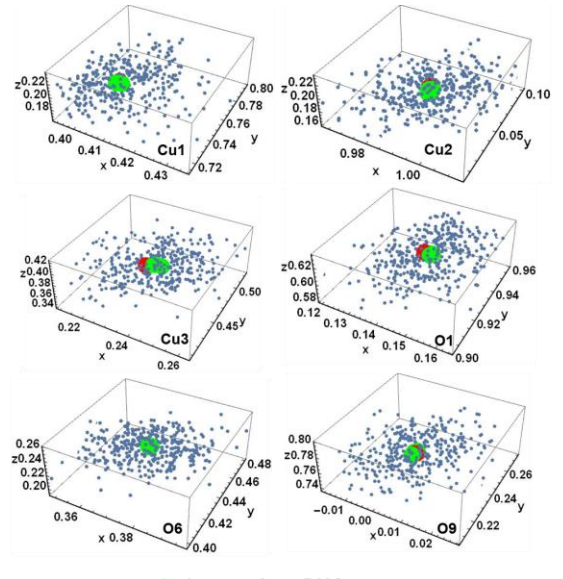

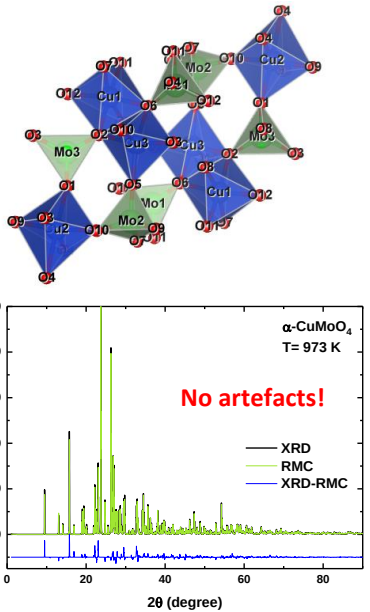

I. Jonane, A. Anspoks, G. Aquilanti, A. Kuzmin, Acta Mater. 179 (2019) 26-35.

High-temperature thermochromic behaviour in α-$CuMoO_4$

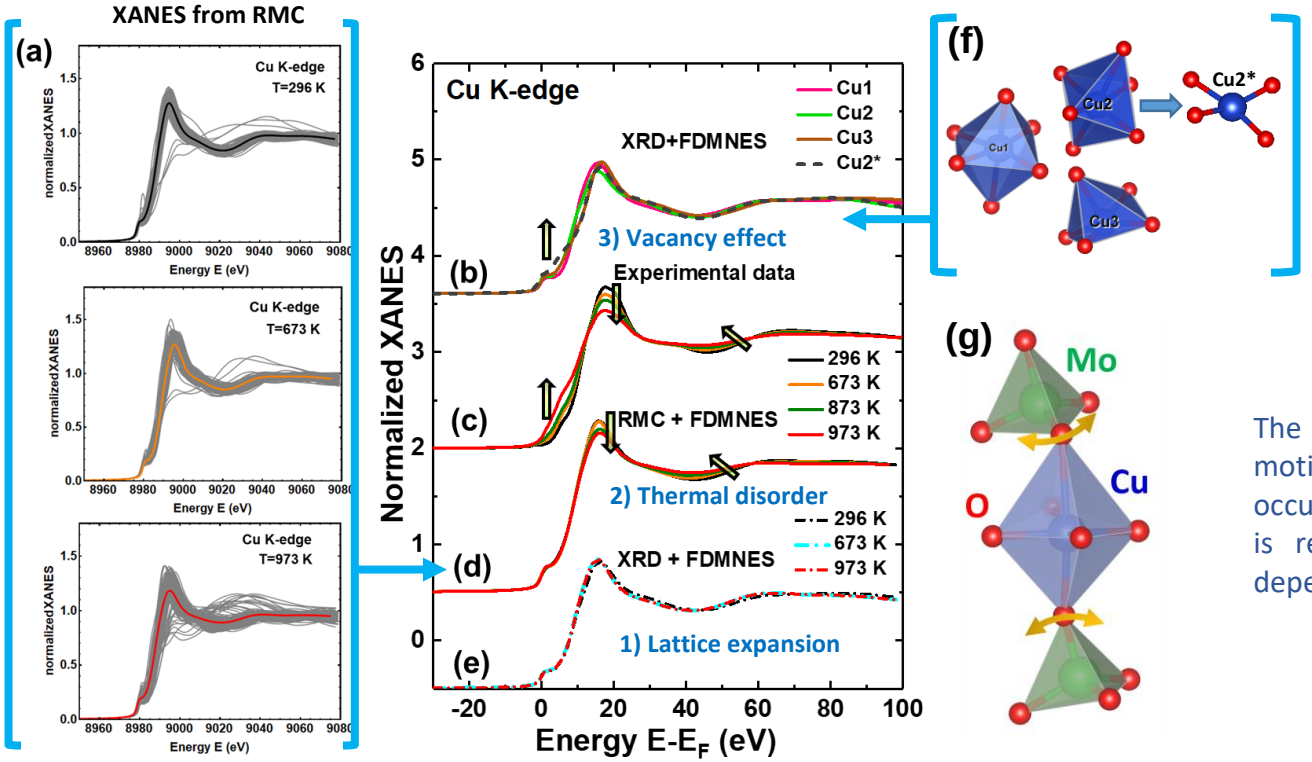

The simulated XANES spectra are in good agreement with the experiment and reproduce the temperature dependence of XANES features.

The reduction of correlation in atomic motion between Cu and axial O atoms occurs upon temperature increase and is responsible for the temperature dependence of the Cu K-edge XANES.

I. Jonane, A. Anspoks, G. Aquilanti, A. Kuzmin, Acta Mater. 179 (2019) 26-35.

High-Entropy Alloys (HEAs)

- Multicomponent alloys without principal component (also known as high-entropy alloys - HEAs) possess many unique properties making them of great interest for materials science [1-2].
- Equiatomic or near-equiatomic HEAs consist of simple crystal structures such as face-centered cubic (FCC), body-centered cubic (BCC), and hexagonal closed-packed (HCP), or their mixtures [3].
- The minor element addition (as aluminum or boron) can cause the increased elastic-strain fields due to atomic size misfit.
- Knowledge of a short-range order (SRO) structure and its dependence on doping is of critical importance for the improvement of HEA properties.

Element selective XAS combined with advanced simulations such as reverse Monte Carlo method.

[1] J.W. Yeh et al., Adv. Eng. Mater. 6 (2004) 299-303.
[2] B. Cantor et al., Mater. Sci. Eng. A 375-377 (2004) 213-218.
[3] D.B. Miracle, JOM 69 (2017) 2130.

Local structure of single-phase Al_x-CrFeCoNi (x=0.3, 3) high-entropy alloys (HEAs)

Structural parameters of as-cast **fcc**- and **bcc**-HEAs determined from SR-XRD data and atomic compositions taken from EDX analysis

	fcc-$Al_{0.3}$CrFeCoNi as-cast ca. 1,900 K	bcc-Al_3CrFeCoNi as-cast ca. 1,973 K
Structural parameters at ambient conditions		
Unit cell parameter, a (Å)	3.572(2)	2.877(2)
Atomic volume, V/Z (Å^3·atom^{-1})	11.39(2) (Z = 4)	11.97(3) (Z = 2)
Sample composition (at.%)		
Al	7.9(2)	44.4(3)
Cr	23.4(2)	13.6(2)
Fe	23.3(2)	14.3(4)
Co	22.2(2)	14.7(2)
Ni	23.2(2)	12.8(9)

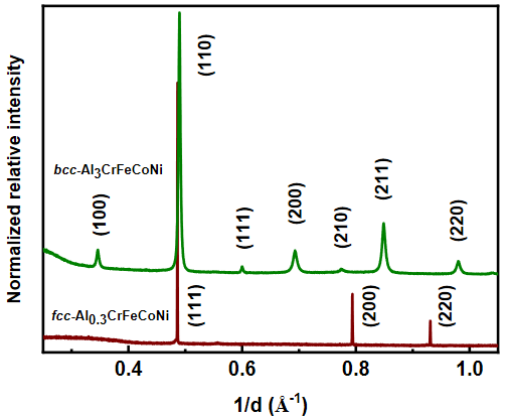

As-cast fcc-structured $Al_{0.3}$-CrFeCoNi (denoted as fcc-HEA) and bcc-structured Al_3-CrFeCoNi (denoted as bcc-HEA) samples (the empirical formulas are given according to energy dispersive X-ray (EDX) analysis of the alloys) were prepared by induction melting above 1900 K in an Ar filled glove-box from powders of pure metals that were loaded in hexagonal boron nitride crucibles.

Large Al atoms act as bcc-phase stabilizer.

A. Smekhova, A. Kuzmin, K. Siemensmeyer, C. Luo, K. Chen, F. Radu, E. Weschke, U. Reinholz, A. Guilherme Buzanich, K. V. Yusenko, Nano Res. (2021), doi: 10.1007/s12274-021-3704-5.

RMC simulations of High Entropy Alloy (HEA)

$Al_{0.3}$-CrFeCoNi

fcc-structured HEA a=3.572 Å

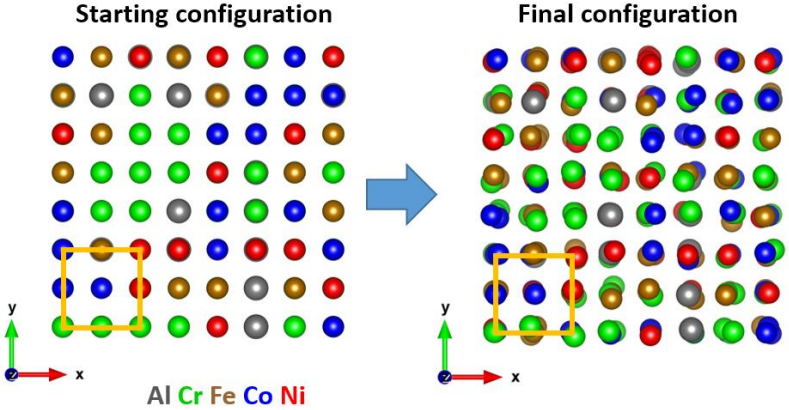

Al_3-CrFeCoNi

bcc-structured HEA a = 2.877 Å

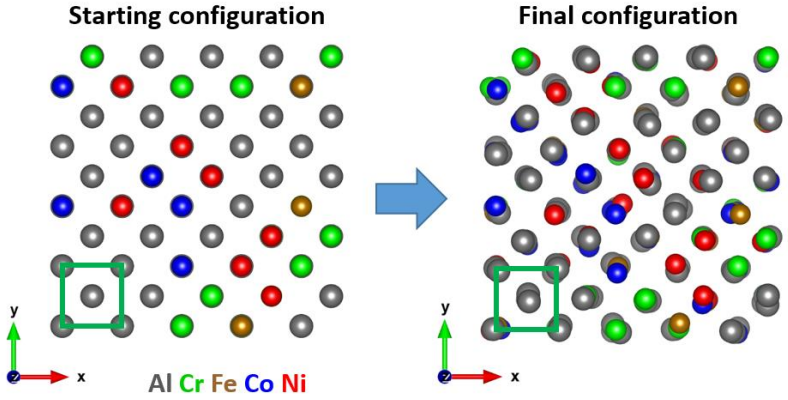

- Supercell 4x4x4 (**fcc**, 256 atoms) or 5x5x5 (**bcc**, 250 atoms) with periodic boundary conditions randomly filled with atoms in the right proportion.
- Several configurations (12 for the fcc-structured HEA and 14 for the bcc-structured HEA) were generated and used in the RMC simulations starting from different (independent) structural models.
- Multiple-scattering effects included up to 4-order.
- Four K-edges (Cr, Fe, Co, Ni) were fitted simultaneously.

RMC fits of High Entropy Alloys with the fcc & bcc lattices

fcc-HEA ($Al_{0.3}$-CrFeCoNi)

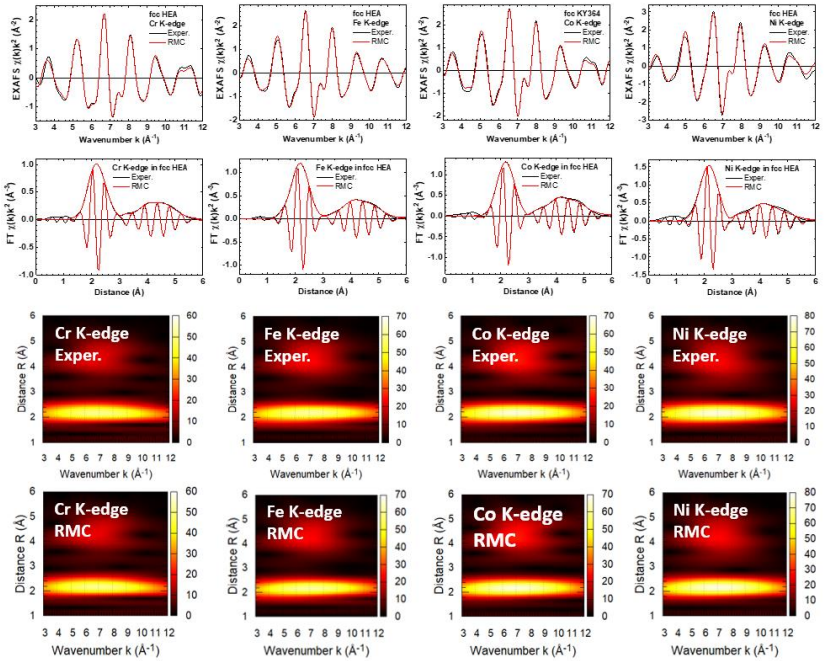

bcc-HEA (Al_3-CrFeCoNi)

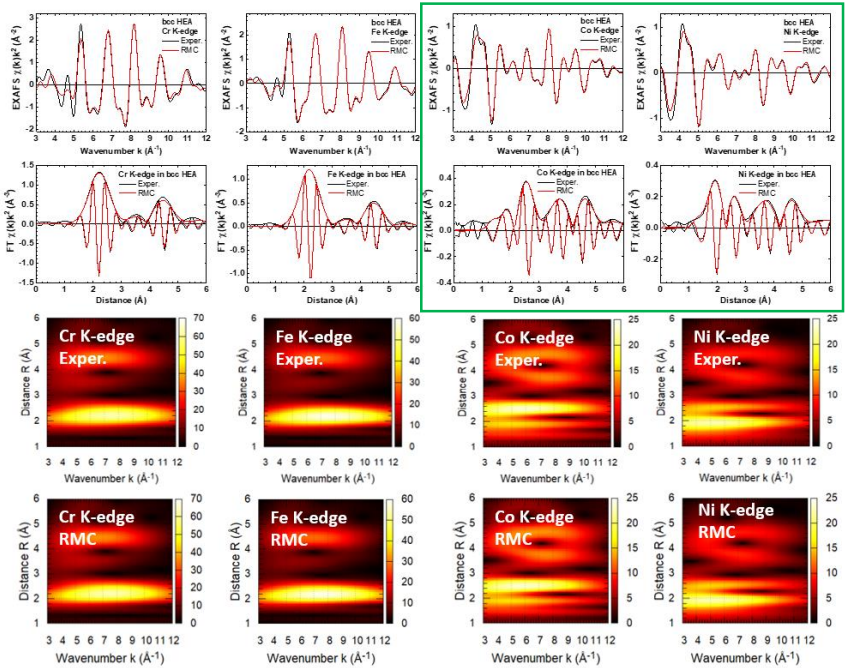

All four edges were fitted simultaneously using the same structural model.

Partial pair distribution functions g(r) for fcc & bcc HEAs

fcc-HEA ($Al_{0.3}$-CrFeCoNi)

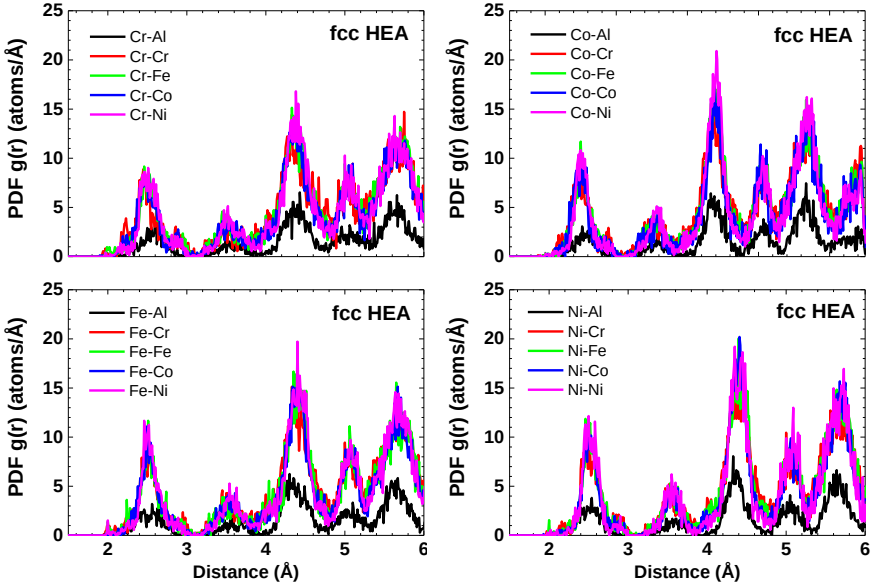

Unimodal distributions

bcc-HEA (Al_3-CrFeCoNi)

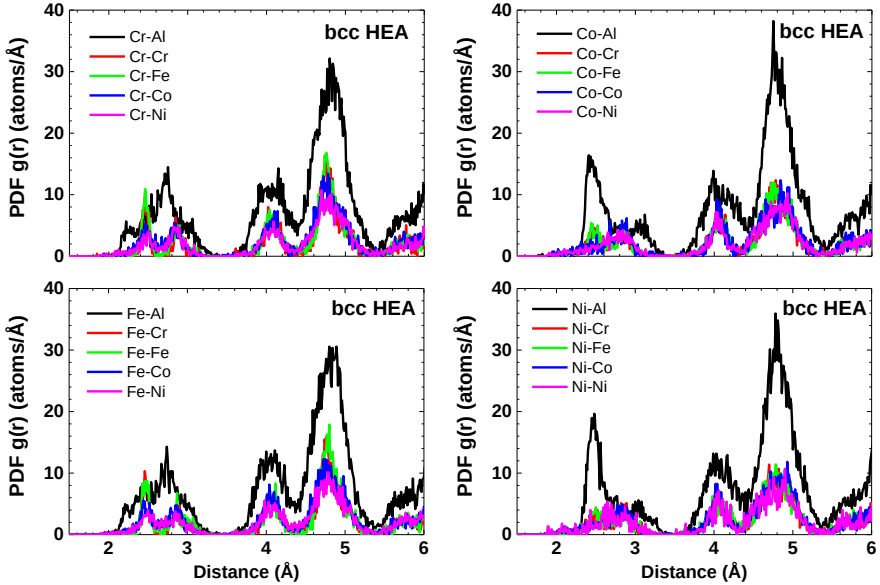

Bimodal distributions

A. Smekhova, A. Kuzmin, K. Siemensmeyer, C. Luo, K. Chen, F. Radu, E. Weschke, U. Reinholz, A. Guilherme Buzanich, K. V. Yusenko, Nano Res. (2021), doi: 10.1007/s12274-021-3704-5.

Analysis of pair distribution functions g(r) for fcc & bcc HEAs

Mean square displacements (**MSD**) determined directly from the coordinates of atoms in the RMC simulation box

	Arrangement in foils	fcc-HEA	bcc-HEA
		MSD (Å)	MSD (Å)
Al	fcc	0.141 ± 0.003	0.212 ± 0.004
Cr	bcc	0.226 ± 0.002	0.161 ± 0.007
Fe	bcc	0.199 ± 0.001	0.155 ± 0.008
Co	hcp	0.181 ± 0.002	0.192 ± 0.007
Ni	fcc	0.162 ± 0.001	0.203 ± 0.004

Mean values of interatomic distances *r* and mean square relative displacements (**MSRD**) σ^2 calculated numerically as moments of PDFs

Atom pair	fcc-HEA		bcc-HEA	
	r(Å)	σ^2(Å^2)	*r*(Å)	σ^2(Å^2)
Cr–Cr/Fe/Co/Ni	2.53	0.038	2.47 2.86	0.010 0.012
Fe–Cr/Fe/Co/Ni	2.54	0.032	2.47 2.87	0.010 0.015
Co–Cr/Fe/Co/Ni	2.53	0.028	2.49 2.85	0.019 0.016
Ni–Cr/Fe/Co/Ni	2.54	0.024	2.52 2.86	0.024 0.015
Cr/Fe–Al	2.55	0.027	2.67	0.065
Co/Ni–Al	2.54	0.022	2.52 3.03	0.016 0.018

- Metals having a lattice type in the bulk similar (dissimilar) to ones of HEA experience less (more) relaxation reflected by MSD.
- Unimodal distribution of distances in fcc-HEA ($Al_{0.3}$-CrFeCoNi) suggests a rather close local structure around all metal atoms in agreement with close shapes of their EXAFS spectra.
- In bcc-HEA (Al_3-CrFeCoNi) all distributions are bimodal but the distribution of Al atoms is broad around Cr and Fe atoms.

A. Smekhova, A. Kuzmin, K. Siemensmeyer, C. Luo, K. Chen, F. Radu, E. Weschke, U. Reinholz, A. Guilherme Buzanich, K. V. Yusenko, Nano Res. (2021), doi: 10.1007/s12274-021-3704-5.

Conclusions

RMC-EXAFS method

- A natural way to include disorder (static and dynamic) into EXAFS simulations taking into account multiple-scattering effects.
- Structural information from the distant coordination shells can be obtained.
- Multi-edge EXAFS analysis is possible and is well suited for complex materials.
- Information on atom-atom and bond-angle distributions and correlations can be obtained.
- Constraints can be easily incorporated to account for information from other experiments (diffraction, total scattering, etc) or chemical/geometrical information (bond-lengths, bonding angles, coordination, energetics, etc).

Thank you for attention!

http://www.dragon.lv/exafs/

https://www.facebook.com/EXAFSLab

FLPP
FUNDAMENTAL AND APPLIED RESEARCH PROJECTS

The financial support provided by the Latvian Council of Science project No. lzp-2019/1-0071 is greatly acknowledged.